Pergamon

Int. J. Heat Mass Transfer. Vol. 37, No. 4, pp. 543–552, 1994

0017-9310/94 $6.00 + 0.00

The effects of supercooling and freezing on natural convection in seawater

ROBERT A. BREWSTER
ADAPCO, 60 Broadhollow Road, Melville, NY 11747, U.S.A.

and

BENJAMIN GEBHART
Department of Mechanical Engineering & Applied Mechanics, University of Pennsylvania, Philadelphia, PA 19104-6315, U.S.A.

(*Received* 12 *August* 1992 *and in final form* 30 *March* 1993)

Abstract—Results of an experimental study of the convective heat and mass transfer processes for downward freezing from a horizontal surface into seawater at 35‰, i.e. at oceanic salinity, are presented here. Liquid supercooling of about 5.0°C was detected at the cooling surface before freezing began. Supercooled water was also detected far from the cooling surface, under some conditions. This supercooling, before freezing, allowed the possibility for density extremum effects to arise under some conditions of low ambient water temperature and large extracted heat flux. After freezing, however, flow visualization revealed that the flow was downward, below the freezing surface. At the high cooling and freezing rate used in these experiments the ice layer and water–ice interface salinities were found to be only weakly dependent on the ice growth rate. Convective heat transfer rates were found to be strongly affected by solute rejection upon freezing.

1. INTRODUCTION

FREEZING in large bodies of water occurs in nature on the surfaces of oceans, lakes and bays. The combined heat transfer associated with heat removal by the environment, and latent heat release at the water–ice interface results in natural convection flows in the water.

A freezing front in saline water rejects solute at the water–ice interface. Seawater has a salinity of about 35‰, where the salinity is defined as the mass, in grams, of dissolved solute per kilogram of solution. Because this salinity is well below the eutectic composition, freezing seawater releases fluid at the water–ice interface which is more dense than the ambient water. The resulting solutal buoyancy force therefore acts downward. This solutal buoyancy force is in addition to the thermal buoyancy force. The direction of the thermal buoyancy force is complicated by the local temperature-dependent density maxima which arise at temperature levels near the freezing point.

The density–temperature relationship for low temperature saline water is similar to that of pure water. Figure 1 shows this relationship for water salinities of 0‰ (pure water) and 35‰ (seawater), at one bar absolute pressure. A supercooled density maximum arises at $t_m \approx -3.4$°C for seawater. The liquidus temperature corresponding to 35‰ salinity is $t_L = -1.9$°C. Therefore, a density extremum does not arise to affect the buoyancy force unless at least 1.5°C water supercooling (cooling below the liquidus temperature) occurs.

The density functions extrapolated below the equilibrium freezing temperatures are indicated by the dashed lines on Fig. 1. It should be noted that density correlations like that of Gebhart and Mollendorf [1], for example, are not known to be highly accurate

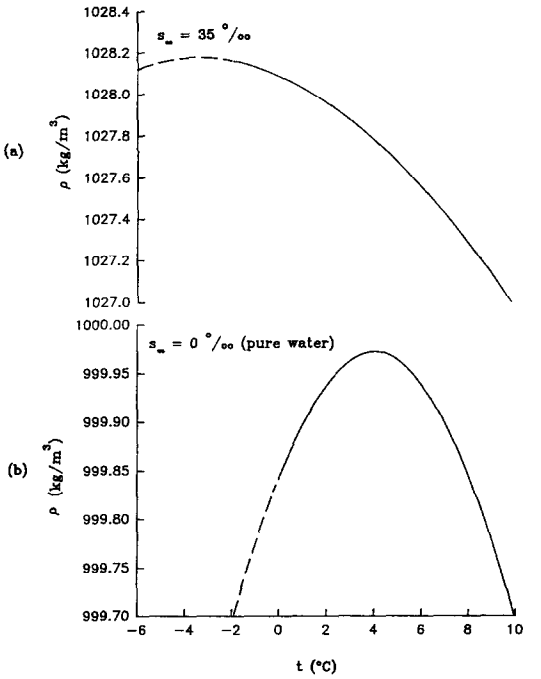

FIG. 1. Density as a function of temperature, at an absolute pressure of 1 bar, for: (a) $s_\infty = 35$‰, (b) $s_\infty = 0$‰ (pure water). Dashed lines represent the density variation below the liquidus temperature.

NOMENCLATURE

g acceleration due to gravity
h heat transfer coefficient
h_{il} specific heat of fusion of seawater
k thermal conductivity of seawater
L length of one side of the cooling surface
L^* $L/4$
Nu_{L^*} Nusselt number
q a constant, 1.8632
q'' heat flux
q''_{conv} heat flux transferred by convection
q''_{ice} $\rho_{ice} h_{il}\,(d\delta/d\tau)$
R density extremum parameter
Ra_{L^*} Rayleigh number
s salinity
t temperature.

Greek symbols
α a constant, $9.3795 \times 10^{-7}(^\circ C)^{-q}$
α_t thermal diffusivity of seawater
β_t thermal expansion coefficient of seawater
β_s saline expansion coefficient of seawater
δ ice thickness
ν kinematic viscosity of seawater
ρ density
τ time
τ_{ice} time at which initial ice formation occurs.

Subscripts
B at the bottom of the aluminum cooling surface
BF before freezing
ice value for the ice
int at the water–ice interface
L liquidus
m value at the extremum
msc maximum value during supercooling
o relevant surface value
∞ ambient value.

Superscripts
$\bar{}$ averaged quantity.

for supercooled waters. Therefore, the dashed curves shown in Fig. 1 represent an approximation.

For saline water, $t_m < t_L$ for salinities greater than 25.5‰, whereas $t_m > t_L$ for salinities less than 25.5‰. This is seen more clearly in Fig. 2, where t_m and t_L are plotted as a function of salinity. The nature of the convective processes which arise may vary greatly across the range of salinities spanning 25.5‰.

Previous studies of the freezing of saline water have not considered the effects of supercooling on convection in a detailed way. Foster [2] visualized flows in artificial seawater with salinities ranging from 19.2 to 34.8‰. About 0.5°C supercooling was observed for salinities less than 25.5‰. There was very little supercooling for salinities greater than 25.5‰. Farhadieh and Tankin [3] observed about 4°C supercooling before freezing. In later experiments [4], the supercooling was suppressed by carborundum particles deposited on the cooling surface.

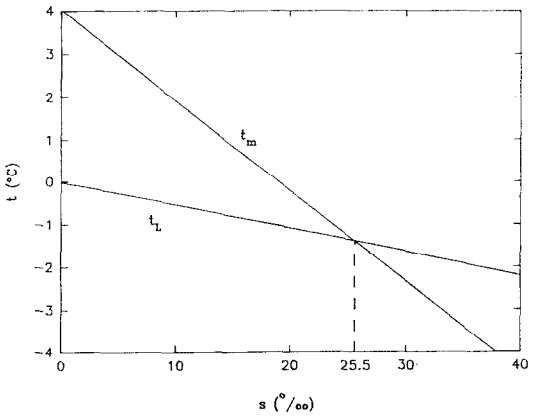

FIG. 2. Density extremum temperature (t_m) and liquidus temperature (t_L), as a function of salinity (s).

The most comprehensive studies of the effects of supercooling on convection during freezing have been in pure water. Brewster and Gebhart [5] examined the effects of supercooling on the onset of freezing and on the resulting convective patterns. They identified three convective flow regimes: upward, buoyancy force reversal, and downward flows. Saito *et al.* [6] have studied the effects of cooling surface finish and cooling rate on supercooling of pure water. Most recently, Nishimura *et al.* [7] have used liquid crystals to determine the effects of supercooling on convection during the lateral freezing of pure water.

The present study is an experimental investigation of downward freezing into a deep layer of cold seawater, using flow visualization and sensor measurements. The flow visualizations reveal the qualitative nature of the buoyancy-induced flows which arise in a cooled layer of seawater, before and after freezing. The effects of supercooling on the convective heat transfer processes before freezing are assessed by measuring the degree of supercooling. These convective processes are further characterized by measurements of heat transfer coefficients, and water–ice interface temperatures.

2. EXPERIMENT

The experimental setup for this study is shown schematically in Fig. 3. Seawater in a 20 gallon hexagonal glass tank was cooled by four thermoelectric

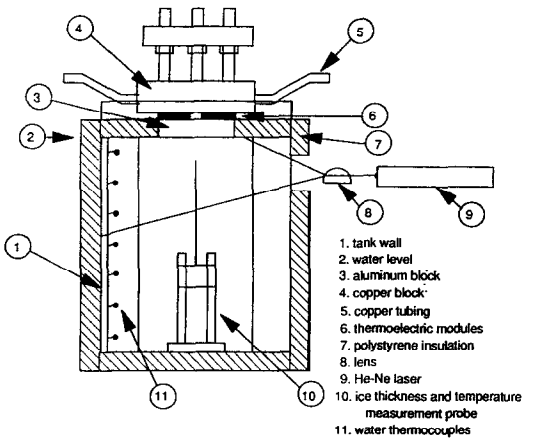

FIG. 3. Schematic of the experimental apparatus, which is housed in a cold room.

cooling modules mounted on top of a 10.87 cm (4.28 inches) square, 2.74 cm (1.08 inch) thick polished aluminum block. The heat was carried away from the thermoelectric modules by ethylene glycol flowing through a copper block bonded to the top of the modules with a thermal epoxy. Teflon-coated polystyrene insulation covered the exposed water surface around the aluminum cooling block. The entire apparatus was housed in a cold room. The water was cooled to the desired temperature for each experiment by setting the cold room temperature, and allowing sufficient time for the water to reach thermal equilibrium with the room. Heat transfer from the water, through the tank walls to the surroundings, was thereby minimized. The total depth of the cooled water layer was 45.7 cm (18 inches).

The aluminum cooling block was instrumented with eight embedded copper–constantan thermocouples very near its bottom and top surfaces. This permitted determination of the heat flux removed from the water and the temperature of the water at the bottom surface of the block. A vertical array of seven thermocouples measured local ambient water temperatures at various depths. Temperature readings were taken every 15 s by a computer-controlled data acquisition system. The accuracy of the temperature measurements is estimated to be $\pm 0.1°C$.

The flow was visualized by laser light scattered by 40 μm diameter pliolite particles. Pliolite is a resin having a density of 1026 kg m^{-3}, which is virtually the same as that of seawater (see Fig. 1(a)). Therefore, pliolite particles are nearly neutrally buoyant in seawater. Light from a 7.0 mW He–Ne laser was spread into a vertical plane by a lens. The pliolite particles scattered the laser light while in this vertical plane. Time exposure photographs were taken by a 35 mm camera controlled by an intervalometer. Each experiment was 30 min long. Ice thickness measurements were made at 2–3 min intervals by a probe raised from the bottom of the tank.

This arrangement was used previously [5] to study natural convection in freezing pure water. However, several modifications were required for experiments in seawater. First, the water–ice interface temperature, t_{int}, had to be measured, since this depends on the water–ice interface salinity, s_{int}, which is not known a priori. The water–ice interface temperature was measured by a special probe designed for this purpose. This probe consisted of a small thermocouple attached to an air-filled plastic bubble. Further details of the probe construction are given in ref. [8]. The probe was tested extensively in pure and saline water, and was found to measure surface temperatures to an accuracy of $\pm 0.1°C$, with an average response time of 0.3 s.

Artificial seawater, prepared using a recipe given by Lyman and Fleming [9], was used in all experiments. Johnson [10] compared 35‰ seawater, prepared using this recipe, to a sample of standard 35‰ seawater obtained from the Institute of Oceanographic Sciences in Wormley, England. Measured electrical conductivities of the two solutions indicated that their salinities agreed to within 0.2‰.

Experiments were performed with an ambient water salinity of 35.0‰. The salinity of the water in the tank was checked daily by measuring its temperature and electrical conductivity, and using the Practical Salinity Scale of 1978, as described by Perkin and Lewis [11]. The accuracies of the salinity measurements are estimated to be ± 0.1‰. If necessary, the water in the tank was adjusted to 35.0‰ by adding either deionized water or a concentrated saline solution, prepared from the recipe.

The salinity of the ice was also determined. At the end of each experiment in which ice formed, the ice was removed from the cooling surface and melted. If the volume of the melted ice was large enough, the salinity of the sample was determined by measuring its electrical conductivity and temperature, and using the Practical Salinity Scale of 1978 [11]. Otherwise, no ice salinity data were obtained for that experiment.

3. FLOW VISUALIZATION

Flow regimes resulting from density extremum effects in cold water may be quantified in terms of a dimensionless density extremum parameter, $R(\tau)$. At 1 bar absolute pressure, $R(\tau)$ is defined by Gebhart and Mollendorf [1] as:

$$R(\tau) = \frac{t_m(s_\infty) - t_\infty}{t_o(\tau) - t_\infty} \tag{1}$$

where t_m is the density extremum temperature, t_∞ is the ambient water temperature, $t_o(\tau)$ is the surface temperature, and τ is time. If no ice is present, then $t_o(\tau)$ is the instantaneous temperature on the bottom face of the aluminum cooling surface, $t_B(\tau)$, where it contacts the water below. If ice has formed on the cooling surface, then $t_o(\tau)$ is the water–ice interface temperature, $t_{int}(\tau)$. Therefore, $t_o(\tau)$ is defined, at any

instant, as the temperature of the cooled solid surface in contact with the water at its upper boundary.

The density extremum temperature, t_m, is a function of salinity, as shown in Fig. 2. The functional relationship between t_m and s at 1 bar absolute pressure was given by Gebhart and Mollendorf [1] as:

$$t_m(s) = 4.029325\,(1 - 0.05265509s) \qquad (2)$$

where s is in ‰ and t_m is in °C.

Convective regimes. Three thermal buoyancy force regimes may be identified, in terms of the parameter R, for a cooled, downward-facing surface. The following discussion applies to $s_\infty = 35$‰, i.e. seawater, when no solutal buoyancy force is present.

In the first buoyancy force regime, $R < 0$. Since $t_o < t_\infty$ (cooled surface), $R < 0$ implies that $t_\infty < t_m$. Then, the buoyancy force is upward everywhere in the water. This is a stable condition for a downward-facing surface. For this situation to arise, the ambient water must be supercooled ($t_\infty < -3.4$°C). Since the entire ambient water would have to be supercooled, this condition would be very unusual, and was not encountered in the experiments.

The second regime is $0 \leqslant R \leqslant 1/2$. This arises if $t_o \leqslant t_m \leqslant t_\infty \leqslant (2t_m - t_o)$. Therefore, t_o must be less than or equal to t_m, which is less than the liquidus temperature. Such a condition requires some supercooling of the liquid. Then, the local buoyancy force is upward in some regions of the water, and downward in other regions, depending on whether the local temperature is less than or greater than t_∞. This is called the buoyancy force reversal regime.

The third regime arises when $R > 1/2$. This occurs when $t_o < t_m < t_\infty > (2t_m - t_o)$, or when $t_m < t_o < t_\infty$. Then, the buoyancy force is downward everywhere in the fluid. This is an unstable circumstance. This regime may arise when $t_o > t_L$, so no supercooling is required. Therefore, this is expected to be the most common occurrence in these experiments. Of course, the addition of a solutal buoyancy during solidification complicates matters. For freezing seawater, the solutal buoyancy force is always downward.

Flow visualizations for an experiment with ambient water temperature $t_\infty = -0.6$°C, and heat flux $\bar{q}''_{B,BF} = 1200$ W m^{-2}, are shown in Fig. 4. The exposure time of each photograph in Fig. 4 is 20 s. The cooling surface is seen at the top-center of each photograph. The heat flux $\bar{q}''_{B,BF}$ is defined as the integrated average of the heat flux through the aluminum cooling block, over the time before freezing begins:

$$\bar{q}''_{B,BF} = \frac{1}{\tau_{cf}} \int_0^{\tau_{cf}} q''_B(\tau)\, d\tau \qquad (3)$$

where τ_{cf} represents the time of the last measurement before freezing, and $q''_B(\tau)$ is the instantaneous heat flux through the aluminum cooling block. After freezing begins, the measured $q''_B(\tau)$ includes the heat of fusion.

Liquid supercooling. Liquid supercooling before freezing was observed in all of the experiments in which freezing occurred. For example, in Fig. 4(a), at $\tau = 2.5$ min, the cooling surface was at $t_o = -4.3$°C ($R = 0.76$), and no ice had formed. The liquidus temperature of seawater is $t_L = -1.9$°C. Therefore, the water adjacent to the cooling surface is supercooled by 2.4°C. In these experiments, the water adjacent to the cooling surface was typically cooled to -6.9°C before ice formed. This represents 5.0°C supercooling (see Fig. 5), about the same supercooling as was found in similar experiments with pure water [5].

Flow development. The vortices seen in Fig. 4(a) are the beginning stages of the development of a downward flow in an initially quiescent ambient water. The water adjacent to the cooling surface becomes more dense and moves downward. Water is entrained inward from below the insulation adjacent to the cooling surface, toward the center of the cooling surface. This is seen in the top corners of Fig. 4(a). The inward flow turns downward after travelling along approximately 1/6 of the width of the cooling surface. The vortex on the far right of Fig. 4(a) turns counterclockwise, while the vortex on the left turns clockwise. These outside vortices drive two counter-rotating inside vortices below the cooling surface.

In time, the two inside vortices disappear. The resulting flow is seen in Fig. 4(b), at $\tau = 4$ min. This flow is essentially a downward plume, with entrainment from the ambient water below the insulation adjacent to the cooling surface. The surface temperature in Fig. 4(b) is $t_o = -5.3$°C, so $R = 0.60$.

The flow at $\tau = 6.5$ min, just before ice forms, is shown in Fig. 4(c). It has changed little from Fig. 4(b). However, the cooling surface temperature is now $t_o = -6.3$°C, and $R = 0.49$. This is just inside the buoyancy force reversal regime.

Ice formation. Dendritic ice has formed on the cooling surface of Fig. 4(d), at $\tau = 8$ min. This type of ice forms after the adjacent water has been supercooled. The flow is still strong and downward. By the end of the experiment, the ice layer has grown much thicker, as seen in Fig. 4(e), at $\tau = 29$ min. The dendrites have disappeared, but there is some waviness of the ice surface.

4. SENSOR MEASUREMENTS

Sensor measurements provided quantitative information about the convective heat and mass transfer processes. The following subsections address specific aspects of the data, including water supercooling, the heat flux necessary to induce freezing, solute rejection, and heat transfer.

4.1. *Liquid supercooling*

Liquid supercooling adjacent to the cooling surface occurred over a wide range of ambient temperature and heat flux conditions. The lowest temperature attained by the cooling surface before freezing for

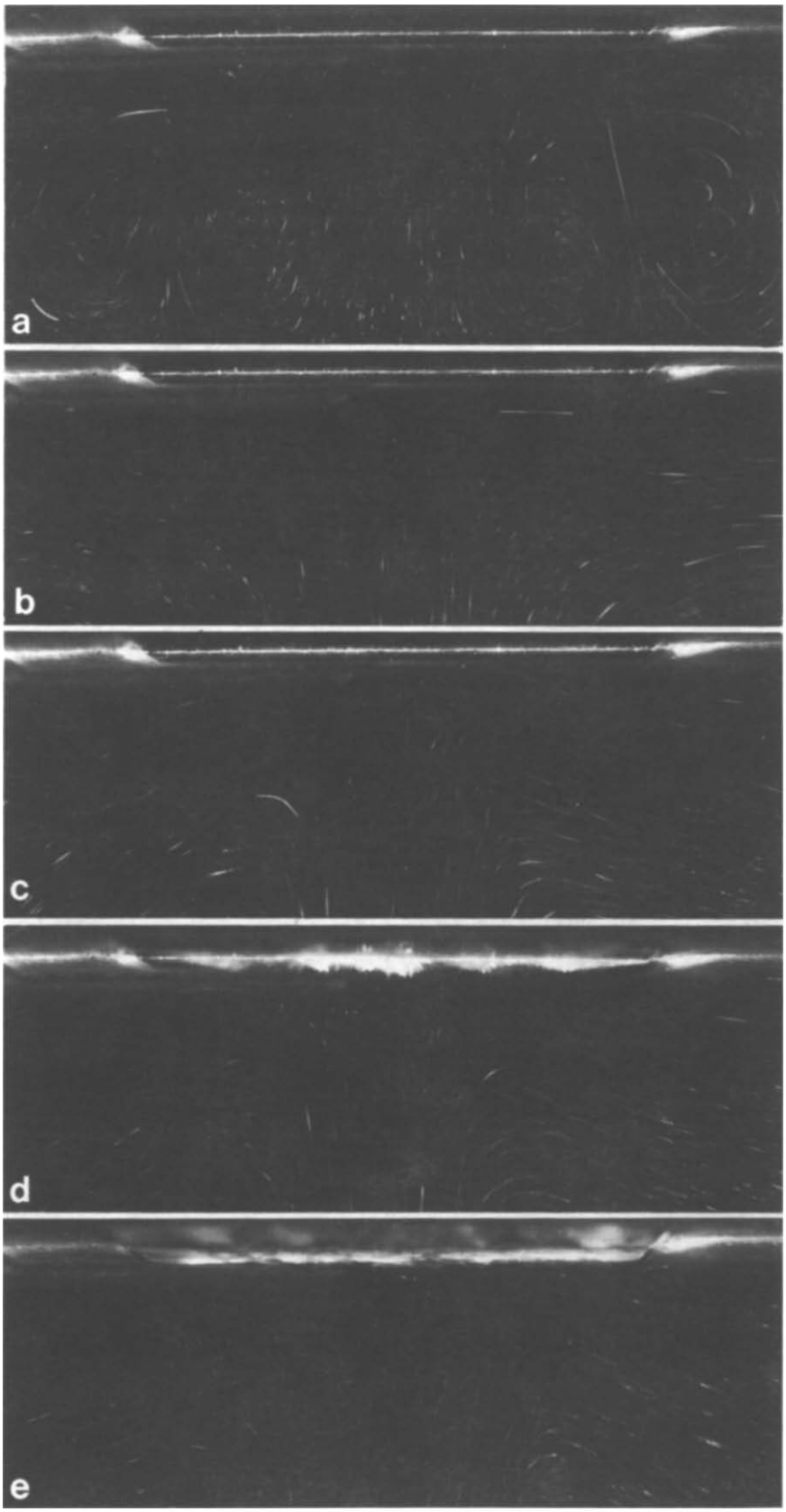

FIG. 4. Flow visualizations for an experiment with $s_\infty = 35‰$, $t_\infty = -0.6°C$, and $\overline{\overline{q''_{R,BF}}} = 1200$ W m^{-2}. Exposure durations in seconds are: (a) 140–160; (b) 220–240; (c) 380–400; (d) 460–480; (e) 1740–1760.

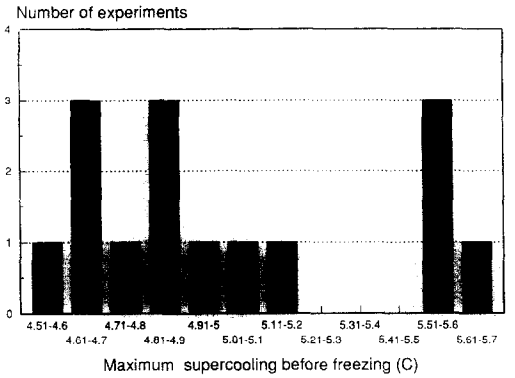

FIG. 5. Maximum supercooling, before freezing began, for experiments in saline water.

any experiment will be referred to as the maximum supercooling temperature, t_{msc}, for that experiment. In this study, it was found that t_{msc} varied somewhat. For example, for an experiment with $t_\infty = 4.5°C$ and $\bar{q}''_{B,BF} = 4530$ W m^{-2}, $t_{msc} = -7.6°C$, while for an experiment with $t_\infty = -0.5°C$ and $\bar{q}''_{B,BF} = 1290$ W m^{-2}, the maximum supercooling temperature was $-6.9°C$.

The histogram in Fig. 5 shows the variation of supercooling before freezing encountered in these experiments. The data of Saito *et al.* [6] for pure water suggest that the variation of supercooling approaches a normal distribution for large sample sizes. However, the sample size here is only 15. The mean supercooling before freezing was 5.0°C, which is very close to the mean of 4.9°C for similar experiments with pure water [5]. The standard deviation of the data in Fig. 5 is 0.4 C.

In some of the experiments, although the cooling surface was at a supercooled temperature throughout much of the experiment, freezing never occurred. The lowest surface temperature maintained until the end of the 30 min experiment without the occurrence of freezing was $t_{msc} = -6.7°C$ for $t_\infty = 4.7°C$ and $\bar{q}''_{B,BF} = 4460$ W m^{-2}.

Nucleation. The variation in the degree of supercooling before freezing apparently arose from nucleation mechanisms on a microscopic level. No attempt was made to control nucleation in these experiments. The following explanation of supercooling and nucleation was formulated by Chalmers [12].

When water of salinity s_∞ is cooled below its liquidus temperature, t_L, clusters of molecules form which resemble the structure of the solid (ice) phase. However, these clusters are not stable unless their radii exceed a critical value. This critical radius is inversely proportional to the supercooling. At any particular temperature below t_L, there is a statistical distribution of cluster sizes. Local nucleation occurs when the radius of the largest cluster exceeds the critical radius. Factors such as cooling surface roughness and water cleanliness also affect the level of supercooling, since they provide nucleation sites.

The roughness of the cooling surface was not changed during the course of these experiments. Particulate matter, such as dust, probably accumulated in the water over time. However, all of the experiments were performed over a span of 28 days. No correlation between the maximum supercooling temperature and the date on which the experiments were performed was found. Therefore, a changing water condition is not thought to be the cause of the variation in t_{msc}. The most likely reason for the variability in t_{msc} would appear to be the occasional occurrence of statistically unlikely cluster sizes.

Supercooled ambient water. Supercooled water was also detected far from the cooling surface under certain conditions. When the water–ice interface temperature was not being measured, the temperature probe remained motionless in the ambient water, approximately 14 cm (5.5 in.) below the cooling surface. It recorded the local temperature in the downward-falling plume visualized, for example, in Fig. 4.

The time variation of this temperature for two experiments is shown in Fig. 6. Figure 6(a) is for $t_\infty = -1.5°C$ and $\bar{q}''_{B,BF} = 970$ W m^{-2}. The gaps in the data for $\tau \geqslant 13$ min correspond to the times when the probe was used to measure the water–ice interface temperature. The data in Fig. 6(a) are characterized by three time periods. In the first period, $0 \leqslant \tau \leqslant 4$ min, significantly cooled water had not reached the probe depth. The temperature is seen to remain relatively constant at about $-1.5°C$. The fluctuations are within the accuracy of the measurements (± 0.1 C).

The temperature drops rapidly at $\tau = 4.25$ min. The plume now carries cooled water down to the probe, the temperature fluctuates rapidly, with a period of

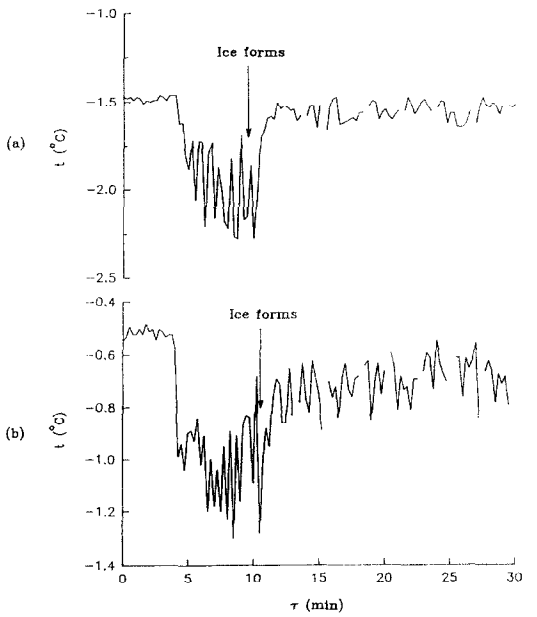

FIG. 6. Transient temperature data at a depth 14 cm below the cooling surface for experiments with: (a) $s_\infty = 35‰$, $t_\infty = -1.5$ C, and $\bar{q}''_{B,BF} = 970$ W m^{-2}; (b) $s_\infty = 35‰$, $t_\infty = -0.5$ C, and $\bar{q}''_{B,BF} = 1370$ W m^{-2}.

about 43 s, about a mean of $-2.0°C$. This temperature is below the liquidus temperature, $t_L = -1.9°C$, about half of the time, indicating that the water being carried down by the plume is supercooled.

The arrow on Fig. 6(a) indicates surface ice formation at $\tau = 9.5$ min. The probe temperature rises abruptly one minute later. Thereafter, it fluctuates about a mean of $-1.6°C$. This sudden rise is caused by the elimination of supercooling when ice forms. The effective cooling surface temperature, $t_o(\tau)$, changed nearly instantaneously from $-6.7°C$ to $-2.2°C$ in this experiment.

Supercooled water was not detected by the probe for ambient water temperatures greater than $-1.4°C$. Figure 6(b) shows data for an experiment with $t_\infty = -0.5°C$ and $\bar{q}''_{B,BF} = 1360$ W m^{-2}. The qualitative behavior is the same as in Fig. 6(a). However, the measured water temperature never drops below about $-1.3°C$. Therefore, no supercooled water reaches the probe depth, although the cooling surface was supercooled to $-7.0°C$ before freezing.

4.2. *Heat flux required for freezing*

It was noted in the introduction above that a density extremum would arise in 35‰ saline water only for at least 1.5°C supercooling. The preceding section indicated that, before freezing, 5.0°C supercooling at the cooling surface was typical. Therefore, density extremum effects may influence the minimum heat flux needed to induce freezing.

In Fig. 7, the average heat flux through the cooling surface before freezing, $q_{B,BF}$, is plotted as a function of the ambient water temperature, t_∞. The filled circles are the experiments in which ice did not form. The open squares are the experiments in which ice did form. The line is an estimate of the dividing line between freezing and non-freezing heat flux levels, as a function of the ambient water temperature.

The dividing line depends upon the convective heat transfer coefficient, the ambient water temperature, and the cooling surface temperature needed to induce ice formation. The scatter of points across the line is due mainly to the variability in the supercooling, as discussed in the previous section. Some of the non-freezing points are well off the line because, in those experiments, the heat flux was not sufficiently large to lower the cooling surface temperature to the (approximately) $-6.9°C$ level needed to induce freezing.

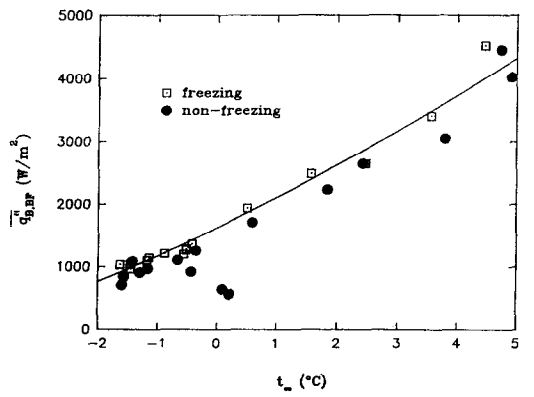

FIG. 7. Minimum heat flux required for freezing as a function of ambient water temperature for experiments at $s_\infty = 35‰$.

The effect of the density extremum on the dividing line in Fig. 7 may be assessed by using the density extremum parameter, R. In particular, since the points along the line are at the maximum supercooling temperature before freezing, the proper surface temperature to use in the evaluation of R is $t_o = t_{msc} \approx -6.9°C$. The value of R at $t_o = t_{msc}$ will be called R_{msc}.

Density extremum effects will arise only if $R_{msc} \leqslant 1/2$, when an upward component of the buoyancy force is present. The lowest value of R_{msc} for any of these experiments was 0.30. This is in the buoyancy force reversal regime ($0 \leqslant R \leqslant 1/2$). However, in pure water studies [5], it was found that the transition point between the upward and downward buoyancy regimes was at $t_\infty = 5.7°C$, corresponding to $R_{msc} = 0.16$. Numerical studies of flows adjacent to horizontal surfaces have shown that this value of R is nearly the same for flows in pure water and in seawater [13]. Therefore, we may conclude that density extremum effects play only a minor role in determining the dividing line in Fig. 7. The flow is very far from being dominated by the upward buoyancy force, as indicated by the strong downflows in the flow visualizations of Fig. 4.

Although supercooling does not affect the heat flux required for freezing through density extremum effects, it does affect this heat flux in a more direct way. Because of the presence of supercooling, the cooling surface needs to be cooled to approximately $-6.9°C$, rather than $-1.9°C$ when there is no supercooling. Then, assuming seawater at 0°C, the heat flux required for freezing would be 3.6 times higher with supercooling than without it. This estimate assumes that the convective heat transfer coefficient is the same for both cases. Of course, this is not really the case, and this estimate will be modified when the convective heat transfer data are discussed.

4.3. *Solute rejection*

Solute rejection by growing ice in seawater provides a downward buoyancy force in addition to the thermal buoyancy force. The saline component of the buoyancy force is expected to be especially significant because of the large density differences caused by salinity gradients, relative to those caused by temperature gradients. That is, $\beta_s \gg \beta_t$, where β_s and β_t are the saline and thermal coefficients of expansion, respectively.

The correlation of Doherty and Kester [14] relates the liquidus temperature of saline water to its salinity. Using the measured water–ice interface temperature, t_{int}, this correlation gives the water–ice interface

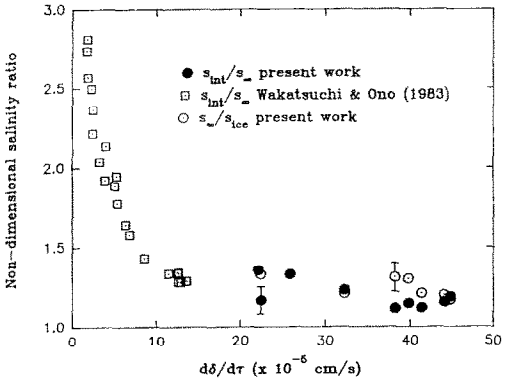

FIG. 8. Non-dimensional water–ice interface salinity and inverse non-dimensional ice salinity as a function of ice growth rate, for experiments at $s_\infty = 35‰$.

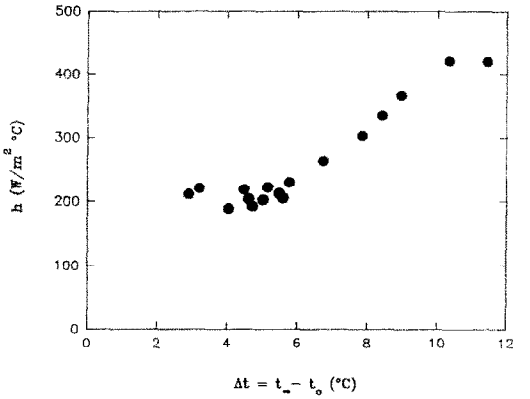

FIG. 9. Steady heat transfer coefficients for non-freezing experiments at $s_\infty = 35‰$.

salinity, s_{int}. However, there are several assumptions that are made in using this procedure.

First, equilibrium conditions at the water–ice interface are postulated, even though freezing at finite rates is not an equilibrium process. Also, the correlation of Doherty and Kester [14] is based on data for water in the salinity range $2 \leqslant s \leqslant 40‰$. Salinities as high as 50‰ were found here, from the interface temperature data. The salinity of the ice formed during the experiments also gave information concerning the solute rejection process.

Water–ice interface salinity. Figure 8 shows the non-dimensional interface salinity, s_{int}/s_∞, as a function of ice growth rate, $d\delta/d\tau$. The filled circles on Fig. 8 are data from the present study. The interface salinity used for each experiment was the average of the inferred values of s_{int} for that experiment. Straight lines were fitted to the ice thickness data, to compute the ice growth rate, $d\delta/d\tau$. These procedures are consistent with the assumption that the water–ice interface salinity correlates with the ice growth rate.

The data of Wakatsuchi and Ono [15], at lower freezing rates, are shown as open squares in Fig. 8. Their data show that s_{int}/s_∞ decreases rapidly with increasing ice growth rate, for low growth rates. At high growth rates, the data from the present study show that an asymptotic value of $s_{int}/s_\infty \approx 1.15$ is approached. For $s_\infty = 35‰$, this asymptotic value corresponds to $s_{int} = 40.3‰$.

The experiments in this study had large ice growth rates because of the supercooling before nucleation. The higher the level of supercooling before freezing, the larger the heat flux needed to induce initial ice formation. Since supercooling always arose before freezing in these experiments, relatively high heat fluxes were needed to cause nucleation. Therefore, when ice did form, it grew at a very rapid rate. Water supercooling before freezing was not reported by Wakatsuchi and Ono [15].

Ice salinity. The open circles on Fig. 8 are the non-dimensional salinity, s_∞/s_{ice}, where s_{ice} is the measured average ice salinity. These data also appear to approach an asymptotic value near 1.15 at high growth rates. This was not expected. Certainly, both s_{int}/s_∞ and s_∞/s_{ice} should be greater than unity, but there is no apparent reason for them to be equal. Although Foster [2] reported experimental values of $s_\infty/s_{ice} = 1.34$ and 1.11, at $s_\infty = 34.8‰$, corresponding ice growth rates were not given.

4.4. *Heat transfer*

Convective heat transfer depends upon the buoyancy force and the vigor of the resulting fluid motion. Since both mass and thermal diffusion arise during solute rejection with freezing, the heat transfer coefficients differ substantially from those when freezing does not occur.

Instantaneous heat transfer coefficients, $h(\tau)$, were calculated from the data using the definition:

$$h(\tau) = \frac{q''_{conv}(\tau)}{t_\infty - t_o(\tau)} \tag{4}$$

where

$$q''_{conv}(\tau) = q''_B(\tau) - q''_{ice}(\tau) \tag{5}$$

and

$$q''_{ice}(\tau) = \rho_{ice} h_{il} \frac{d\delta(\tau)}{d\tau} \tag{6}$$

where ρ_{ice} is the density of the ice, and h_{il} is the specific heat of fusion of the seawater. Note that $q''_{ice}(\tau)$ is the rate of latent heat release due to ice formation per unit area of the cooling surface. Of course, $q''_{ice}(\tau) \equiv 0$ for non-freezing experiments, and for freezing experiments at times before nucleation had occurred.

For non-freezing experiments, $t_o(\tau) = t_B(\tau)$, the temperature at the bottom of the cooling surface. For freezing experiments, $t_o(\tau) = t_{int}(\tau)$, the measured water–ice interface temperature.

Steady heat transfer coefficients for non-freezing and freezing experiments are plotted in Figs. 9–11. These data were inferred by taking the arithmetic mean of the instantaneous heat transfer coefficient, $h(\tau)$, computed from the data for each experiment.

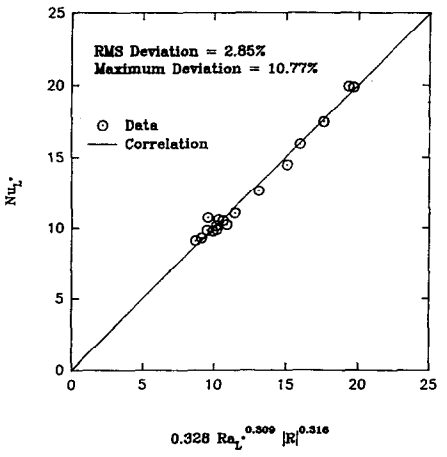

FIG. 10. Comparison of correlation with data for non-freezing Nusselt numbers.

For the non-freezing experiments, the data were averaged over the final 10 min of each experiment. For the freezing experiments, the average was over the final 2 min. The instantaneous $h(\tau)$ did not vary substantially over these periods.

Non-freezing data. These data are shown in Fig. 9. The flattening of the data at low Δt is thought to be due to increasing density extremum effects, as the increasing upward thermal buoyancy force component more effectively opposes the downward buoyancy force.

The role of density extremum parameter, R, on the convective heat transfer coefficient, h, is shown in the form of a non-dimensional correlation in Fig. 10. The Rayleigh and Nusselt numbers are defined as:

$$Ra_{L^*} = \frac{g\alpha|t_\infty - t_0|^q L^{*3}}{\nu\alpha_t} \tag{7}$$

$$Nu_{L^*} = \frac{hL^*}{k} \tag{8}$$

respectively, where g is the acceleration due to gravity, $\alpha = 9.3795 \times 10^{-7}$ $(°C)^{-q}$ and $q = 1.8632$ are constants in the density correlation of Gebhart and Mollendorf [1], and ν, α_t and k are the kinematic viscosity, thermal diffusivity and thermal conductivity of the seawater, respectively. The length scale was chosen as $L^* = L/4$ where L is the length of one side of the square cooling surface. This length scale was suggested by Goldstein *et al.* [16] as appropriate for natural convection from horizontal surfaces, when the buoyancy force is away from the heat transfer surface.

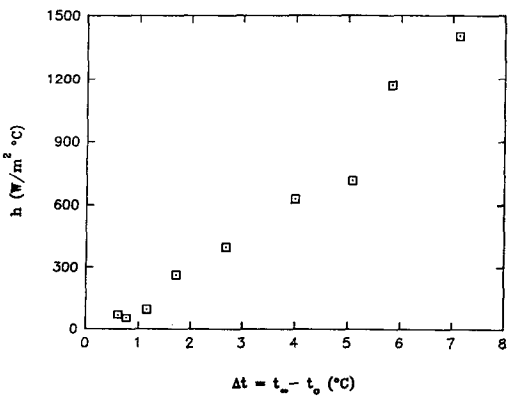

FIG. 11. Steady heat transfer coefficients for freezing experiments at $s_\infty = 35‰$.

The correlation given in Fig. 10 fits the data very well. The r.m.s. deviation is less than 3%. One data point has a deviation of nearly 11%, however, all other data points have deviations of less than 4.5%. The correlation is valid over the ranges $0.38 \leqslant R \leqslant 1.25$ and $5.3 \times 10^4 \leqslant Ra_{L^*} \leqslant 7.9 \times 10^5$.

We can now modify our earlier estimates of the heat flux required for freezing with and without supercooling. Using the correlation with $t_\infty = 0°C$, we can find that the heat transfer coefficient is 1.8 times as large when the surface temperature is $-6.9°C$ (supercooling) as when it is $-1.9°C$ (no supercooling). Then, the heat flux required for freezing is twice as large when supercooling is present. Therefore, supercooling in bodies of seawater is a very large impediment to the freezing process.

Freezing data. The steady-state heat transfer coefficients for freezing are given in Fig. 11. The freezing data are at smaller $\Delta t = t_\infty - t_0$ than the non-freezing data (see Fig. 9). This arises because supercooling is eliminated when nucleation occurs. This increases the effective surface temperature, t_0, and therefore decreases Δt. The freezing heat transfer coeffcients are much larger than for the non-freezing experiments, at the same Δt. The saline component of the buoyancy force which arises after freezing substantially increases the vigor of the flow. The thermal buoyancy force component is then much smaller.

5. CONCLUSIONS

Flow visualizations, ice salinity, and local sensor measurements have been used to study the effects of supercooling and freezing on natural convection in seawater. Experiments were performed over a range of ambient water temperatures and extracted heat fluxes.

Density extremum effects were generally not important. Flow visualizations indicated that the flow was downward before and after freezing began. No buoyancy force reversal effects were seen, even though about 5.0°C supercooling occurred before freezing. Supercooled liquid was also detected far below the cooling surface for ambient water temperatures below $-1.4°C$.

Rejection of solute occurs at the water–ice interface during freezing. Measured water–ice interface temperatures allowed the calculation of the water–ice interface salinity. These results, at high freezing rates, followed the trend of the data of Wakatsuchi and Ono [15]. The data indicate that the ratio of the water–ice interface salinity to the ambient water salinity

approaches an asymptotic value of 1.15, at the high ice growth rates encountered here. The ratio of the ambient water salinity to the salinity of the ice appeared to approach the same asymptotic value of 1.15.

Heat transfer coefficients for freezing and non-freezing experiments were computed from the data. Density extremum effects did play a role in heat transfer before freezing at low water temperatures. These effects are caused by the large supercooling of the liquid before freezing. The cooling surface temperatures which arose lie on the dashed portion of Fig. 1(a). The heat flux required for freezing was estimated to be two times as large as it would be if supercooling was not present.

The heat transfer coefficients for the freezing experiments were generally very much higher than those for the non-freezing experiments. The vigor of the flows after freezing is greatly increased by the strong downward saline component of the buoyancy force, which is caused by the solute rejection at the water–ice interface.

Acknowledgements—The authors wish to acknowledge support for this work under National Science Foundation grant CTS 91-19829.

REFERENCES

1. B. Gebhart and J. C. Mollendorf, A new density relation for pure and saline water, *Deep-Sea Res.* **24,** 831–848 (1977).
2. T. D. Foster, Experiments on haline convection induced by the freezing of sea water, *J. Geophys. Res.* **74,** 6967–6974 (1969).
3. R. Farhadieh and R. S. Tankin, Interferometric study of freezing sea water, *J. Geophys. Res.* **77,** 1647–1657 (1972).
4. R. Farhadieh and R. S. Tankin, A study of freezing sea water, *J. Fluid Mech.* **71,** 293–304 (1975).
5. R. A. Brewster and B. Gebhart, An experimental study of natural convection effects on downward freezing of pure water, *Int. J. Heat Mass Transfer* **31,** 331–348 (1988).
6. A Saito, Y. Utaka, S. Okawa, K. Matsuzawa and A. Tamaki, Fundamental research on the supercooling phenomenon on heat transfer surfaces—investigation of an effect of characteristics of surface and cooling rate on a freezing temperature of supercooled water, *Int. J. Heat Mass Transfer* **33,** 1697–1709 (1990).
7. T. Nishimura, M. Fujiwara, N. Horie and H. Miyashita, Temperature visualizations by use of liquid crystals of unsteady natural convection during supercooling and freezing of water in an enclosure with lateral cooling, *Int. J. Heat Mass Transfer* **34,** 2663–2668 (1991).
8. R. A. Brewster, Experimental studies of natural convection effects on downward freezing of cold pure and saline water and stability of mixed convection flow adjacent to a vertical isothermal surface, Ph.D. Thesis, University of Pennsylvania, Philadelphia, Pennsylvania (1988).
9. J. Lyman and R. H. Fleming, Composition of sea water, *J. Mar. Res.* **3,** 134–139 (1940).
10. R. S. Johnson, Transport from a melting vertical ice slab in saline water. M.S. Thesis, State University of New York at Buffalo, Buffalo, New York (1978).
11. R. G. Perkin and E. L. Lewis, The practical salinity scale 1978: fitting the data, *IEEE J. Ocn. Engng* **5,** 9–16 (1980).
12. B. Chalmers, *Physical Metallurgy*, pp. 237–238. Wiley, New York (1959).
13. I. El-Henawy, B. Gebhart and N. D. Kazarinoff, Multiple steady-state solutions for horizontal buoyant flows in cold water, *Int. J. Heat Mass Transfer* **29,** 1655–1667 (1986).
14. B. T. Doherty and D. R. Kester, Freezing point of seawater, *J. Mar. Res.* **32,** 285–300 (1974).
15. M. Wakatsuchi and N. Ono, Measurements of salinity and volume of brine excluded from growing sea ice, *J. Geophys. Res.* **88,** 2943–2951 (1983).
16. R. J. Goldstein, E. M. Sparrow and D. C. Jones, Natural convection mass transfer adjacent to horizontal plates, *Int. J. Heat Mass Transfer* **16,** 1025 (1973).